Nelson, L. J., & Smith, R. A. (2019). Fibre direction and stacking sequence measurement in carbon fibre composites using Radon transforms of ultrasonic data. *Composites Part A: Applied Science and Manufacturing*, *118*, 1-8. https://doi.org/10.1016/j.compositesa.2018.12.009

Fibre direction and stacking sequence measurement in carbon fibre composites using Radon transforms of ultrasonic data

L. J. Nelson[a,*], R. A. Smith[a]

[a] *Department of Mechanical Engineering, University of Bristol, Bristol, BS8 1TR, UK*

Abstract

Stacking sequence and, more generally, fibre orientation, are critical parameters in fibrous composite materials since they govern mechanical performance. This paper presents a method, based on the ultrasonic pulse-echo non-destructive technique, that can map the stacking sequence in unidirectional carbon-fibre composites. In-plane fibre orientation is measured using a Radon-transform method applied to local 2D images extracted from the 3D dataset formed from a 2D scan of pulse-echo responses. The ability to align these local 2D images to the plies in the region being assessed makes this technique suitable even in laminates where out-of-plane ply wrinkling is present. The Radon-transform method is shown to provide interpretable stacking-sequence maps, allowing ply lay-up sequence and both in-plane waviness and out-of-plane wrinkling to be visualised and quantified.

Keywords: A. Layered structures, B. Directional orientation, D. Non-destructive testing, D. Ultrasonics

1. Introduction

1.1. Requirement

Stacking sequence, the order in which the 0°, 90°, +45° and −45° unidirectional plies are ordered in a composite laminate, is an important design consideration. This sequence is carefully chosen to impart a desired mechanical performance to the part, so deviations from the design intent are important to identify. An incorrectly manufactured laminate can suffer reduced strength [1, 2] and changes in its response to impacts [3, 4] if the intended sequence is not achieved. A typical post-production quality-assurance non-destructive inspection using ultrasonic methods will identify defects such as inclusions, delaminations and porosity, but not the stacking sequence of the plies. There is a growing awareness that this aspect of composite parts needs to be assured. This paper presents a method, based on an ultrasonic pulse-echo non-destructive inspection, that can provide a visual map quantifying the stacking sequence to meet this requirement.

1.2. Non-destructive methods

Two methods have emerged over recent years that are able to provide sensitivity to fibre features in carbon-fibre reinforced polymer composites, these are X-ray CT [5–11] and ultrasound [12–16].

In X-ray CT the trade-off between spatial-resolution and component size makes it unsuitable for large, laminar components that are common in various industry sectors, such as aerospace and automotive, since the required imaging resolution can not be achieved [17]. Further, the low contrast between the carbon fibres and typical resin systems makes datasets difficult to analyse [11, 17]. In such cases ultrasonic inspection is preferred.

Pulse-echo ultrasonic inspection involves interrogating a material with pulses of ultrasonic-frequency acoustic waves. Those waves reflected from the material that are received at the probe are used to image surface and sub-surface features in the material. By raster-scanning a probe over a carbon-fibre reinforced polymer (CFRP) laminate surface and storing the ultrasonic reflections (A-scans) at each location, a 3D dataset is obtained. Research has shown that in laminated composite materials the often-ignored low-amplitude reflections from the thin pure-resin inter-ply layers can be used to map ply locations [12, 18], and also to image fibre tow features [14]. Therefore, as a non-destructive technique it has the capability to acquire datasets with potential for fibre-orientation and stacking-sequence measurement.

The influence of the probe's frequency characteristics such as peak-frequency and bandwidth, and spatial characteristics such as focal depth and F-number, although now broadly understood [12, 19], have a marked influence on the resulting dataset. Attenuation of the ultrasonic pulse also leads to a depth limit, although the used of depth-dependent amplification can overcome this to a degree. Ultrasound has some unique benefits that make it a desirable imaging modality for CFRP laminates. Firstly, it is well suited to large laminar components because, when deployed in pulse-echo mode, it requires access to only one side of the part being inspected and can readily be

*Corresponding author
Email address: luke.nelson@bristol.ac.uk (L. J. Nelson)

extended to array-based acquisition to achieve high scan rates. Pulse-echo ultrasound datasets can also achieve high depth resolution, dictated by the time-domain sampling of the waveform and probe bandwidth, and this resolution is independent of the in-plane resolution, governed by the scan pitch and probe beam-width. This independence provides resolution tuning in the required depth dimension allowing accurate evaluation of plies and fibres without unnecessarily increasing resolution in lateral dimensions.

Only recently has the interaction between an ultrasonic pulse and a laminar CFRP composite reached a stage where successful acquisition of datasets to reveal fibre and ply features is becoming routine. This interaction is now briefly summarised.

1.3. Ultrasonic pulse-echo interaction with CFRP

Analytical modelling work [18–20] has provided a thorough understanding of the interaction of ultrasound with a uni-directional monolithic composite. Such composites contain a number of plies, on which fibres of a common orientation are constrained, each ply being separated from its neighbours by a thin (typically 5-50 μm) resin-rich layer. Being resin-rich, this layer has a different acoustic impedance to the composite (fibre and resin) layer, and thus produces a weak ultrasonic reflection at the composite-to-resin and resin-to-composite interfaces. Since the resin layer is very thin in comparison to the ultrasonic wavelength these two reflections combine to give a single reflection that is the superposition of the two interface reflections [21]. This resin-rich inter-ply layer contains an imprint, in the form of thickness variations, of the fibre and fibre-tow architecture of the ply before it and after it. In the typical range of frequencies used for ultrasonic inspection the reflection amplitude at the resin layer is, to a first approximation, proportional to the layer thickness, thus an image of the reflection amplitude from the resin layer corresponds to a resin-layer thickness map, and contains visual information on the fibre-tow architecture of the two plies that contact it, as seen in Fig. 1. This is the basis for the sensitivity to fibre orientation in an ultrasonic pule-echo dataset.

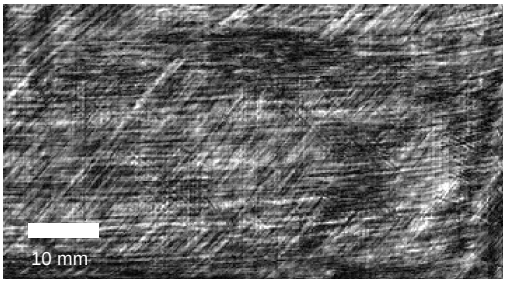

Figure 1: An in-plane (x-y) image showing the instantaneous amplitude from a fixed time-of-flight within the 3D dataset. Amplitude variations (black corresponds to low amplitude) result from the thickness variations imparted on the inter-ply resin layer by the fibres and fibre-tows in each contacting ply.

It is possible to enhance the weak reflection by selecting an ultrasonic probe with a frequency that coincides with the ply's resonance-frequency. A further consideration, revealed by modelling [12], is that the probe should have a broad-band nature, with a Q-factor close to 1, such that the probe bandwidth spans the resonance frequencies in a typical composite in which plies can vary in thickness, particularly in regions of ply wrinkling. To image the fibre features with sufficient spatial resolution a focused probe is a necessity. Ultrasound will not resolve individual fibres since they are too small (typically 5-7 μm), but will resolve the fibre tows, composed of many thousands of fibres, provided the beamwidth is smaller than the fibre-tow width. To achieve this, focused probes with a -6 dB beam diameter in the order of the fibre tow spacing, approximately 0.5 mm, are required.

1.4. Fibre-orientation measurement

Many techniques for detecting fibres and measuring their orientation are seen in the literature [9], spanning many scientific fields. Examples include techniques based on structure tensor [22–28], Radon transform [29–32], Fast Fourier Transform (FFT) [14, 33–38], rotated filter [39–44], and image moment [45–47] methods.

Whilst the structure tensor has been previously used by the authors to successfully determine out-of-plane *ply* orientation from ultrasonic data [22], it is not an appropriate method for in-plane *fibre* orientation. Unlike the smoothly varying ply-orientation field, the fibre-orientation field is likely to feature abrupt changes each side of a resin layer, for example switching from a -45° to a $+45^\circ$ fibre angle. Therefore, the resin-layer reflection-amplitude image will contain impressions of these two fibre orientations. There may also be influences from other ply interfaces, for example, an amplitude image formed at a ply centre will contain an impression of the ply interface above and below it and will therefore contain information from three plies. For these reasons an amplitude image from a given depth in the composite laminate will contain multiple fibre orientations (see Fig. 1). The structure-tensor method is not suitable for determining orientations in image data in which more than one orientation exists, so it is necessary to explore alternative approaches.

Methods based on rotated filters, FFTs and Radon transforms are all appropriate techniques since they can be used to generate an angular distribution from a 2D image containing multiple orientations. Further processing allows the dominant orientation to be determined (for example, the angle associated with the peak in the distribution). For this study a Radon-transform method is developed that determines fibre orientation from 2D images taken from the 3D ultrasonic dataset. Such images can be taken in the x-y slice-plane if the plies are known to be parallel to a component with a flat front surface, or can be realigned to the plies in the region being assessed if the plies are not flat. The realignment of the 2D-imaging

plane is likely to be required in laminates where ply wrinkling is present, or the laminate exhibits a curvature. The out-of-plane ply-orientation map needed to achieve this realignment can be assessed using the technique presented in [22].

1.5. Paper overview

This paper's technical contribution begins in Section 2 in which the novel process of determining the stacking sequence of a CFRP laminate using a Radon-transform technique is described. In Section 3 the ultrasonic data acquisition from a 23-ply laminate, and pre-processing applied prior to performing the technique, are described. Stacking-sequence results are presented and discussed in Section 4, followed by a summary and presentation of the main conclusions in Section 5.

2. Stacking-sequence method

2.1. Ultrasonic scanning

The first stage in determining stacking sequence is to acquire a pulse-echo ultrasonic scan from a CFRP laminate. The scan must cover a 2D area of the component, thus a means to translate a probe over the area is required. For example, an *x-y* raster scan using an immersion tank, a water-jet system, or a recirculating-water probe head (dripless bubbler) system would all be suitable methods. Single-element probes and array probes, both linear and 2D arrays, are suitable if the -6dB focal spot size is circular to avoid imaging bias, and of a suitably small diameter so that fibre-tow features can be imaged.

2.2. Instantaneous amplitude and phase

Once digitised, the Hilbert transform is used to obtain the analytic signal of each pulse-echo waveform acquired from the scanning system [12]. From this, the instantaneous-amplitude and instantaneous-phase datasets are generated.

Although only the amplitude data is used for fibre orientation analysis, phase data is used to perform the alignment and segmentation pre-conditioning stages, described in Section 3.4. Additionally, phase data allows a contextual overlay to be generated which is used in combination with the stacking-sequence map to locate ply interfaces. A beneficial outcome of applying the phase overlay is that double plies of the same orientation can be distinguished.

2.3. Fibre-orientation mapping

The basis of determining the fibre orientation is the Radon transform [48], a 2D image transform. At each pixel location in the 3D ultrasonic-amplitude data-volume, a local 2D image is extracted. Ideally, this 2D image will be aligned to the local ply structure on which the fibres are constrained. Typically it is sufficient to obtain the 2D image aligned to the *x-y* scanning plane, since, for a flat laminate, the plies on which the fibres are constrained also lie in this plane. However, in components featuring inclined plies, such as tapered components, and in regions exhibiting non-planar plies, such as at ply-wrinkling defects, the successful measurement of *fibre* orientation may also require the determination of the *ply* orientation. This does not require any further data acquisition, as measuring ply orientation can be achieved using the same acquired ultrasonic data-set, as will be shown later in Section 4.3.

A Radon transform is applied to each 2D instantaneous-amplitude image. The result, itself a 2D image, is subsequently reduced to a 1D angular distribution, from which the dominant orientation is calculated. By repeating this process at all locations in the volumetric amplitude data a 3D dataset of local in-plane fibre orientation is obtained.

The Radon transform, R, for a two-dimensional image function $f(x, y)$ maps an image to its integral on lines defined by angle θ and offset r, as shown in Fig. 2 (a), and is defined by Eq. 1 [49].

$$R(r,\theta) = \int\int f(x,y)\delta(x\cos\theta + y\sin\theta - r)\,dx\,dy \qquad (1)$$

In which δ is the Dirac delta function, which is zero except when $r = 0$. The presence of the term $\delta(x\cos\theta + y\sin\theta) - r$ in the definition of the Radon transform forces the integration of $f(x, y)$ along the line $x\cos\theta + y\sin\theta - r = 0$, where r is the nomal-distance to the line from the origin, and θ is the angle between that same normal and the x-axis, as shown in Fig. 2(a).

The Radon transform is perhaps best understood by way of an example. For this purpose a 12 mm square region from an *x-y* near-surface cross-section through an ultrasonic-amplitude dataset is used. Fig. 2(b) shows this region, which has been windowed using a circular mask to limit the fibre information to a maximum radius from the centre pixel. Two example projections are also presented, one at $\theta = 90^\circ$ and one at $\theta = 0^\circ$. The Radon transform, Fig. 2(c), is composed of such projections, from $\theta = 0^\circ$ to $\theta = 180^\circ$.

To determine the fibre angle, it is necessary to reduce the 2D Radon-transform image to a 1D angular distribution. Two methods are seen in the literature, both of which quantify the contrast variation of each projection, which is highest when the projection is aligned to line (fibre) features in an image. The first [32, 50–52] measures the variance of the projections, whilst the second [29] quantifies the gradients. This paper uses the gradient method, as follows. Firstly, the projection bias of the Radon transform is removed by dividing each projection point by the number of pixels from which is was formed. The angular distribution, Fig. 2(d), is then obtained by summing the absolute gradients, calculated using a central-difference kernel, for each projection. Such a measure is highly sensitive to large gradient changes, as seen for the 90° projection in Fig. 2(b). This measure is higher the closer the fibre-tow impressions are in the image, so this method tends to filter out the low spatial frequency variations, which is an

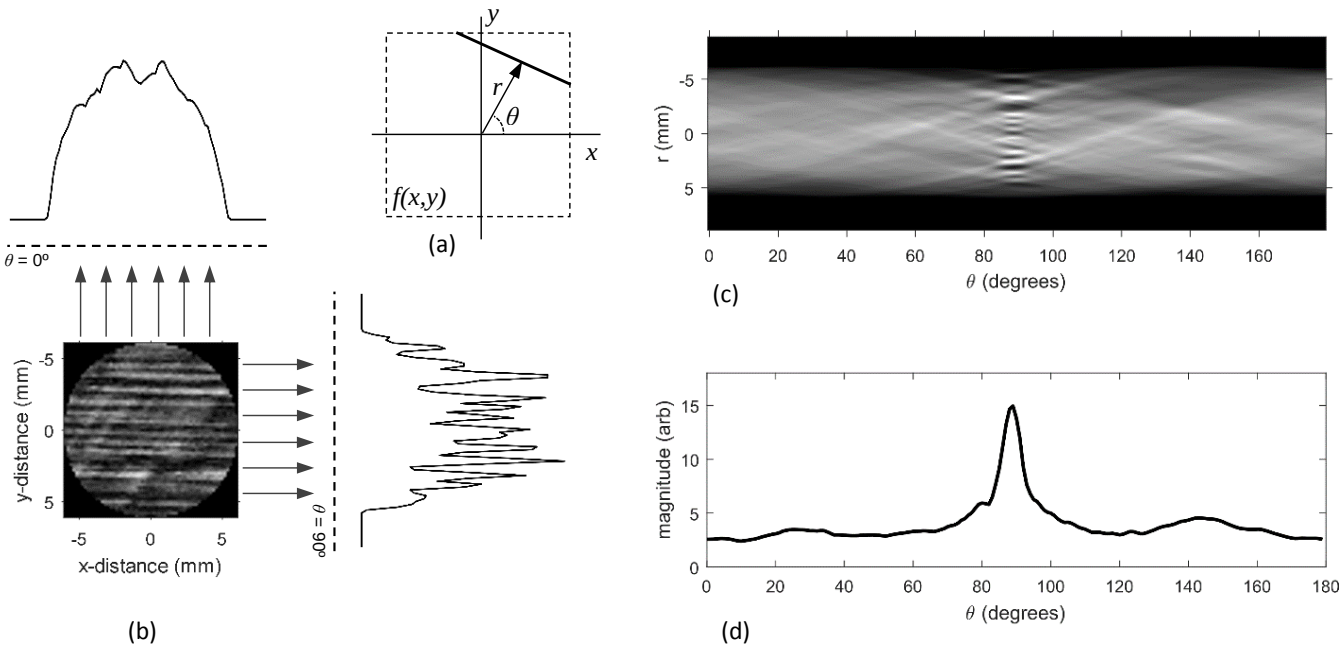

Figure 2: Overview of the Radon transform process showing (a) the parameterisation of a line in the 2D image function $f(x, y)$, showing the normal-distance r from the origin, and the angle θ between the normal and the x-axis, (b) the windowed 2D image region and two example projection profiles at $\theta = 90^\circ$ and $\theta = 0^\circ$, (c) the Radon transform formed from such projections, and (d) the angular distribution of the image in (b) calculated from the Radon transform.

advantage over the variance method. The dominant fibre angle in the image is measured as that coinciding with the maximum amplitude of the angular distribution. The maximum amplitude is also recorded so it can be used as a confidence measure to allow exclusion of angle measurements in regions where there is no significant fibrous content. Such regions produce a low maximum amplitude in the distribution. By performing this process at each pixel location in the 3D amplitude dataset, a 3D map of local in-plane fibre angle is obtained, together with a 3D map of a confidence-related parameter.

This process is now demonstrated by applying it to an ultrasonic pulse-echo dataset obtained from a CFRP laminate with a known stacking sequence.

3. Ultrasonic data acquisition and pre-processing

3.1. CFRP sample details

The carbon-fibre laminate studied in this paper is known to contain both ply wrinkling and fibre waviness, thus is an ideal laminate for this study. It has 23 plies with a stacking sequence, confirmed by optical microscopy of polished edges (see Fig. 3 for an example), and X-ray CT, of:

$$[+45/0/-45/90/-45/0/+45_2/0_2/-45/\overline{90}]_s$$

Each ply is nominally 125 μm spacing, resulting in a laminate that is approximately 3 mm thick.

3.2. Ultrasonic pulse-echo data acquisition

The laminate was scanned in an ultrasonic immersion tank using a spherically focused polymer immersion transducer with a specified frequency (f) of 20 MHz, but a measured centre frequency of 18 MHz (Fig. 4) because these polymer probes have a very flat, broad spectral response. This centre frequency probably reduces further due to frequency-dependent attenuation in the composite.

The transducer had an element diameter (D) of 5 mm and a focal length (F) of 38.1 mm (1.5 inches). In a typical composite laminate with a sound velocity (c) of approximately 3000 ms^{-1} a -6 dB pulse-echo beam diameter (BD_{-6dB}) at focus of 1.2 mm can be expected, as given by Eq. (2) [53].

$$BD_{-6dB} = \frac{1.032Fc}{fD} \tag{2}$$

The poly-vinylidene flouride (PVDF) active element gives the probe a broadband frequency response so that the resonance of the ply structure can still be excited even when the ply thickness changes, a necessity in the case where ply wrinkling is present. A time-domain and frequency-domain pulse-echo probe response is presented in Fig. 4.

Key probe parameters obtained from Fig. 4 are: a peak frequency of 18.6 MHz, a -6dB bandwidth of 12.7 MHz, and a -6 dB centre frequency of 18.1 MHz. The instan-

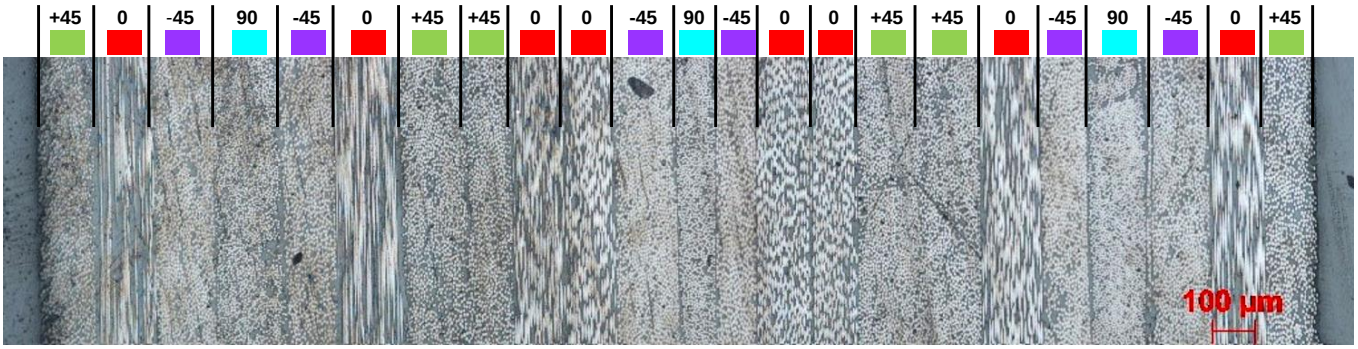

Figure 3: An optical micrograph of the full thickness of a polished 0° edge from the 23-ply lamiante. This, and polished edges at other angles, confirmed the stacking sequence as $[+45/0/-45/90/-45/0/+45_2/0_2/-45/\overline{90}]_s$, as shown in the figure. The sequence has also been colour-coded to match later images of stacking sequence measurement.

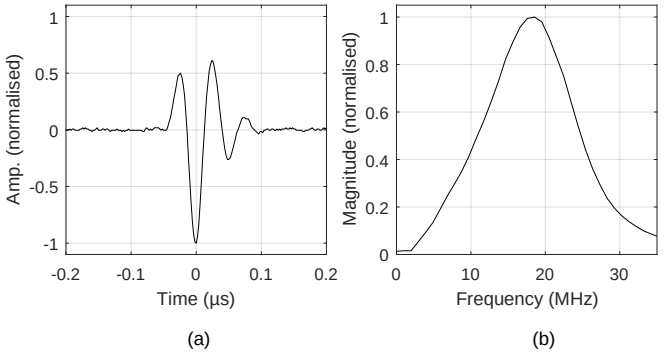

Figure 4: (a) Time domain and (b) frequency domain waveform characteristics of the immersion probe used in this study, as measured from a reflected pulse from a brass plate set at the focal distance of the probe.

taneous phase at peak instantaneous amplitude (ϕ_0) was measured to be -3.04 radians.

A raster scan of the entire laminate surface was obtained with a scan pitch of 0.2 mm in x and y directions with the probe's focus set at the mid-plane of the laminate. Attenuation with depth into the sample was partially overcome by using a time-varying gain that aimed to bring all ply reflections to a similar amplitude prior to being digitised using an 8-bit A/D converter at a sampling rate of 500 MS/s. The digitised 3D dataset was imported into MATLAB to perform all further analysis.

3.3. Instantaneous amplitude and phase

Instantaneous amplitude and phase were calculated by applying the Hilbert transform to the RF pulse-echo waveforms. Prior to using the instantaneous phase a filtering stage was employed as follows. The model-predicted fundamental ply resonance frequency for the laminate is 12 MHz, with a second harmonic occurring at 24 MHz. Thus the probe, with a peak frequency of 18.6 MHz, could preferentially excite the second harmonic if the plies become slightly thicker (bringing the resonances down in frequency). In this second-harmonic scenario the phase advances by two full rotations, or 4π radians, per ply. To obtain the ideal phase response of one rotation per ply, a 15 MHz low-pass filter was used to remove the high-frequency component. The instantaneous amplitude was kept unfiltered to retain the high frequencies, associated small focal-spot size, and hence the high sensitivity to fibre-tow features.

3.4. Alignment and segmentation

Prior to performing any orientation analysis it is important to correct for sample misalignment during scanning. The process followed is briefly described below, with a more detailed description available in [22].

Firstly, the times-of-flight corresponding to the front- and back-surface of the component in the waveform are determined. Instantaneous-amplitude data is used initially to define these locations (in time) because the peak instantaneous amplitude has been shown by modelling [18] to coincide with the time-of-flight to these interfaces. To improve robustness of this measurement, the phase corresponding to the front surface, ϕ_0, and rear surface, $\phi_0 - \pi$, in the vicinity of the amplitude-predicted locations, is located. Here, ϕ_0 is the phase at peak amplitude of the input pulse-echo pulse, which can be estimated from the phase at peak amplitude from the front-surface reflection of the composite laminate [18]. These amplitude-guided phase-derived surface-location measurements are used to define the front- and back-surface component times-of-flight in the 3D waveform data.

Because the surface of the laminate was known to be slightly curved it was not appropriate to use a traditional 'interface gate' to align the waveform data, as this would force the image of the surface to become flat, and distort the true geometry of the laminate. To avoid this, the predicated front-surface location was used to calculate a plane-of-best-fit to the surface, which was used to time-shift each A-scan so that the front surface lies nominally in the x-y plane, but retains its curvature and local undulations.

The curvature of the laminate also made it necessary to account for the dissimilar sound velocities in the coupling medium (water), and composite, to avoid distortion. To give a true image of the component's structure it is important to apply the correct velocity to each portion of the waveform. In this paper, velocities of 1480 ms^{-1} and 3043 ms^{-1} were used for the water and composite respectively.

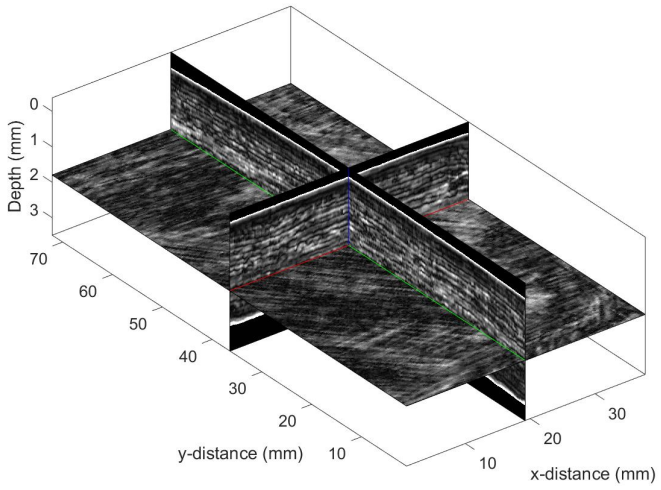

Figure 5: Orthographic projection slices in the 3D instantaneous-amplitude data volume after alignment and segmentation. The bright bands of high amplitude arise from the ultrasonic reflections from the inter-ply resin layers at these locations.

The three-dimensional aligned, scaled and segmented amplitude data, cross sections through which are shown in Fig. 5, reveal ply structure as bright bands in the out-of plane (x-$z$and y-z) slices, and fibre features on the in-plane (x-y) slice. It is on this dataset that the fibre-orientation analysis described in Section 2.3 was performed, the results of which are now presented.

4. Results and discussion

4.1. Fibre angle map

A cross-section through the resulting in-plane fibre-orientation map obtained from the Radon transform process is shown in Fig. 6(a). Circular disk regions of 4 mm (20 pixels) in diameter, from the x-y plane, were analysed to obtain the local fibre angle at each pixel location. The wrapped colour-scale selected to display the fibre angle result produces bands of uniform colour in the x-z cross-section that allow a visual confirmation of stacking sequence. Starting with the central cyan band at a depth of 1.5 mm, corresponding to a ply with 90° fibres, it is possible to see the balanced nature of the laminate by the symmetry in colour bands above and below this central ply.

The ply order is correctly identified throughout the depth of the laminate, with the exception of the first and, to a lesser extent, the last ply. These are known to be 45° plies, and thus should appear as green bands at these locations. It is thought that the dominance of the front and back-surface reflections, which are large relative to the inter-ply resin-layer reflections as result of the large acoustic-impedance difference between the laminate and water, is responsible for this effect by masking the required resin layer reflections.

Although the order of the plies can be determined from the image in Fig. 6(a), the cross-section does not provide the means to identify double plies with the same fibre angle. Double plies are known to exist in four locations in the sequence; the two mid-laminate green bands at 1 mm and 2 mm are double 45° plies, whilst the two red bands towards the centre of the laminate are double 0° plies. It is possible to identify these correctly as double plies using the instantaneous-phase data, Fig. 6(b), in the process described in Section 4.2.

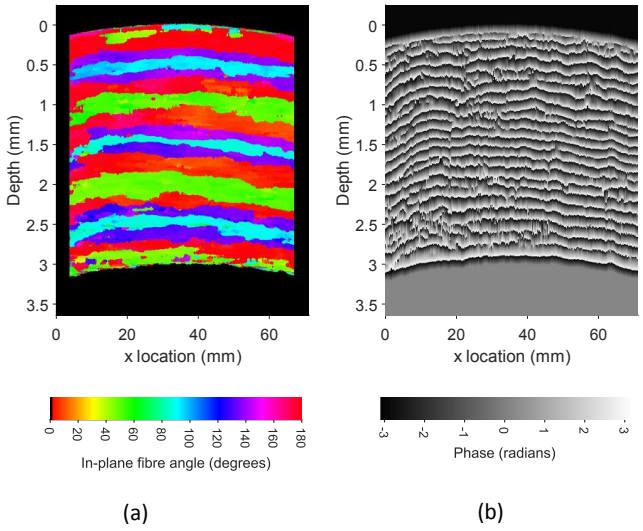

Figure 6: Cross-sectional slices through (a) the stacking-sequence dataset, and (b) the instantaneous-phase dataset. The stacking sequence was obtained by applying the Radon-transform technique to ultrasonic instantaneous-amplitude data. The analysis region was a disk 4 mm (20 pixels) in diameter in the x-y plane.

4.2. Ply location overlay

Modelling results predict that the ply interfaces will attain a phase value of $\phi_0 - \frac{\pi}{2}$. By mapping these locations in the phase cross-section as black, whilst setting all other phase values transparent, the location of the resin layers, and the plies they separate, becomes apparent. An 'interface map' image such as this can be used as an overlay on the stacking-sequence cross-sections to provide ply-location information, as shown in Fig. 7, where the phase-derived black lines delineate the ply boundaries.

Ply boundaries predicted from the phase data align well to the transitions of dominant angle, providing evidence that the location best-suited to determine fibre orientation is the ultrasound response from a ply centre. The

purpose of this phase overlay is to identify the double plies, which is successfully achieved, as evidenced by a ply-boundary appearing at the centre of each double-ply location.

The ply boundaries do not appear as continuous lines as would be expected. There are many locations where the resin-layer phase value is not achieved, resulting in discontinuities in the ply-boundary lines. In addition, there is a degree of apparent noise present in the phase overlay, a result of the resin-layer location (thickness) being affected by the fibre-tow imprint. It is possible to apply a smoothing method prior to determining the ply boundaries to improve these detrimental aspects, resulting in the cross section shown in Fig. 8. The smoothing method is now described.

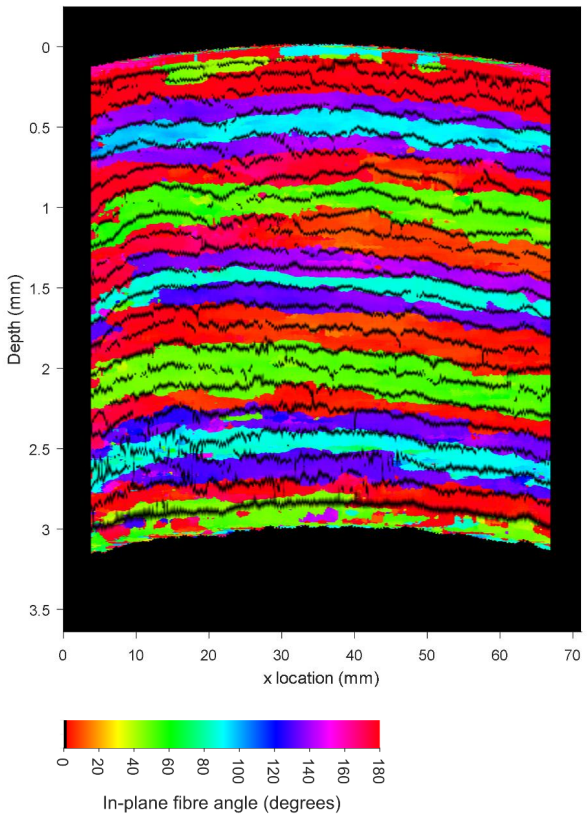

Figure 7: Stacking-sequence cross-section image (colour) from Fig. 6(a), with a phase-overlay (black) derived from Fig. 6(b) to locate the ply boundaries.

4.3. Smoothing and ply-aligned analysis

The approach taken to remove the inconclusive resin-layer locations, potentially a result of fibre-tow induced resin-layer thickness variations, is to smooth the phase data. Smoothing is restricted to a 2D disk profile in the 3D data to prevent blurring the phase data. It is necessary to align the 2D disk regions to the plane of the plies in the location being smoothed, rather than being locked to the x-y scanning plane. Thus, to achieve the proposed 'guided smoothing' it is a requirement to obtain the local *ply* orientation dataset that can be used to guide the smoothing process.

A local ply-orientation map was obtained using the structure tensor method previously developed [22], applied to the instantaneous-phase 3D dataset. Key parameters for this analysis are the smoothing scale and the integration scale, which were set at zero (no smoothing) and (4, 4, 4) pixels, or (0.8, 0.8, 0.012) mm respectively. This ply-orientation data was used to align a 2 mm diameter (20 pixel) 2D smoothing-disk parallel to the plies in the phase data. Smoothing was applied to the disk in the form of a mean, applied to both the cosine and sine of the phase to avoid errors at the phase wrap locations, followed by recombining to produce a ply-aligned smoothed wrapped-phase 3D dataset.

Fig. 8 presents a cross-section through this dataset, with a grey-scale mapping that makes ply boundaries show as black, overlaid on a colour fibre-orientation cross-section. The fibre orientation dataset from which the cross-section in Fig. 8 was taken was obtained using the Radon transform method as previously, but instead of 2D images being locked to the x-y plane, as in Fig. 7, the images are aligned to the local ply orientation. This may be considered as 'guided fibre analysis' and has the benefit of providing more reliable results in regions where plies do not align to the x-y plane. Such locations occur in wrinkled regions, and also potentially in tapered components. An example of the improvement achieved can be seen by examining the mid-plies at a depth of 1.5 mm at an x-location of 10 mm. Comparing Fig. 8 to Fig. 7, a more robust measurement of fibre angle is obtained in this location.

The smoothed-phase data gives a clearer indication of the ply boundaries with fewer discontinuities. However, many ply-boundary discontinuities still remain. There are at least two likely causes for these discontinuities.

Firstly, there are locations, such as in the double 45° ply (green) at a depth of 1 mm, where the ply appears to become thinner, a result of the ply wrinkling that is present. This thinning increases the resonance frequency of a single ply so it now falls outside the probe bandwidth. The ultrasound in this location now preferentially excites a thickness-resonance of the squashed double-ply, whose resonance frequency has increased so that it now falls within the bandwidth of the probe. Thus the phase advances one full rotation for this thin double-ply, instead of two rotations, and it appears as a single ply.

A second cause of discontinuities is related to the fibre tows. This is difficult to show in image form but it is possible, when interactively visualising the 3D data volume shown in Fig. 9, from which Fig. 8 is obtained, to observe that the location of certain discontinuities track the fibre orientation of the ply in which they occurs. An example location is seen in Fig. 8 at the deeper double 45° ply (green) at a depth of 2 mm and an x-location of 25 mm.

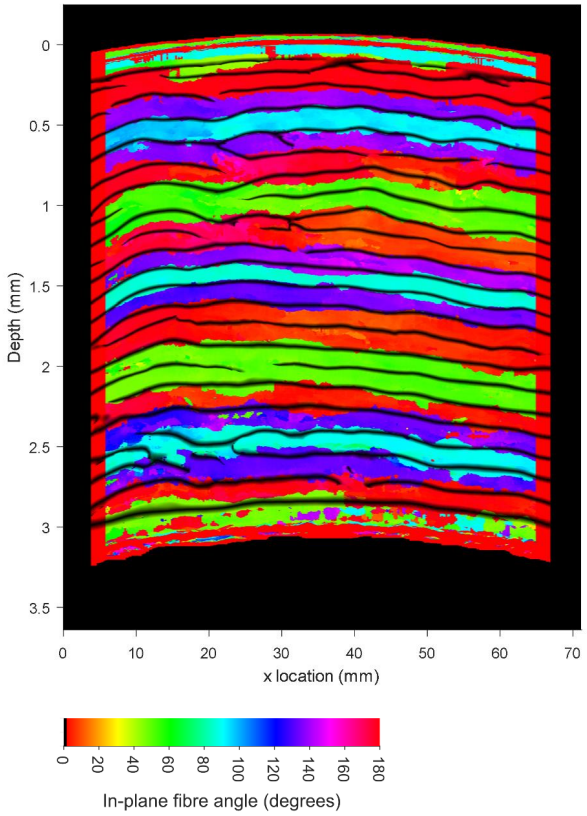

Figure 8: Stacking-sequence cross-section image (colour) obtained by a guided-processing Radon-transform method. A phase-overlay (black), obtained from a guided-smoothing process, locates the ply boundaries.

During layup and consolidation of a composite laminate it is possible for fibre tows within a ply to become separated so that a resin-rich seam forms. This is particularly likely to occur in locations of in-plane fibre waviness, and out-of-plane ply wrinkling, due to the movement of the fibre-tows that must occur during the formation of these features. At these resin-rich locations, the ultrasonic reflections do not combine in the same way as at a typical resin layer because the resin layer becomes a full ply in thickness [18]. The result is the instantaneous amplitude at this location is significantly reduced, leading to a poorly defined phase. This effect is believed to be responsible for many of the phase-tracking discontinuities in Fig. 8.

The focus of this paper has been on determining the stacking sequence in CFRP laminates, and a colour-scale spanning the full orientation-space has been chosen to allow stacking sequence to be visualised. However, observation of the in-plane slices in Fig. 9 shows potential for the identification and quantification of smaller deviations from the intended fibre angle, such as when in-plane fibre waviness is present. The exploration of the use of this method for quantifying and visualising fibre-waviness is a logical extension, and will be the subject of future work.

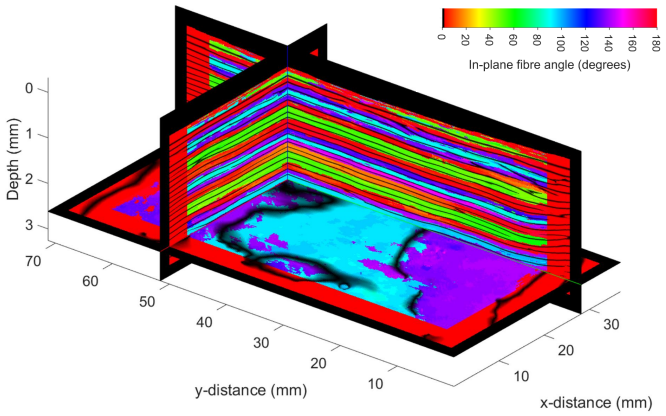

Figure 9: Orthoganal slices through the 3D stacking-sequence dataset presented in Fig. 8 in which the ply-interface overlay (black) has been obtained from a guided-smoothing process applied to the phase data, and the in-plane orientation measurement obtained from a guided fibre-analysis process.

5. Summary and conclusions

This paper has presented a method for non-destructively determining the stacking sequence, or in-plane fibre angle, of a CFRP laminate. The method relies on acquiring an ultrasonic pulse-echo scan from a laminate, followed by application of the Hilbert transform to access the instantaneous-amplitude and instantaneous-phase datasets. A Radon-transform based method has been developed and applied to the instantaneous-amplitude data, resulting in a fibre-orientation distribution for a local region. From this distribution the dominant angle is measured and assigned as the in-plane fibre angle. By repeating this process at each pixel location a 3D map of in-plane fibre angle is generated.

Cross sections through the fibre orientation data can be used to deduce the stacking sequence, with additional ply-boundary location information, obtained from the instantaneous-phase data, overlaid to aid in the detection of double plies.

By using the local ply-orientation information obtained from a previously-developed structure-tensor method, it is possible to orientate the Radon transform fibre-angle analysis to align with the plies, achieving improved results in regions where plies deviate from the x-y scanning plane. The guided-processing principle has also been applied to smooth the fibre-tow induced noise in the phase data. These processing techniques lead to significantly improved results, thus simplifying the identification and quantification of the stacking sequence. The remaining discontinuities in the ply boundary data are thought to be caused by real effects like resin-rich areas between fibre tows, which act like the ply drops seen in [18].

Future work will focus on the identification and removal of phase discontinuities occurring at thin plies and at resin rich locations caused by fibre-tow separation, and on the identification and mapping of in-plane fibre-waviness features.

6. Acknowledgements

The authors would like to acknowledge Miss Maria Zilidou for acquiring optical micrographs and Dr. Christina Fraij for undertaking X-ray CT scans that confirmed the stacking sequence of the CFRP lamiante used in this paper. This work was supported by the Engineering and Physical Sciences Research Council of the UK under Grant No. EP/K037315/1. Data generated during this project can be accessed at the University of Bristol data repository, data.bris, at https://doi.org/10.5523/bris.228hf6zaj8sha2v0y6w4i45jf7.

References

[1] M. R. Piggott, The effect of fibre waviness on the mechanical properties of unidirectional fibre composites: A review, Composites Science and Technology 53 (2) (1995) 201–205. doi:10.1016/0266-3538(95)00019-4.

[2] K. Potter, B. Khan, M. Wisnom, T. Bell, J. Stevens, Variability, fibre waviness and misalignment in the determination of the properties of composite materials and structures, Composites Part A: Applied Science and Manufacturing 39 (9) (2008) 1343–1354. doi:10.1016/j.compositesa.2008.04.016.

[3] E. Fuoss, P. V. Straznicky, C. Poon, Effects of stacking sequence on the impact resistance in composite laminates - Part 1: parametric study, Composite Structures 41 (1) (1998) 67–77. doi:10.1016/S0263-8223(98)00036-1.

[4] M. A. Caminero, I. García-Moreno, G. P. Rodríguez, Damage resistance of carbon fibre reinforced epoxy laminates subjected to low velocity impact: Effects of laminate thickness and ply-stacking sequence, Polymer Testing 63 (2017) 530–541. doi:10.1016/j.polymertesting.2017.09.016.

[5] A. Bhattacharya, C. Heinzl, A. Amirkhanov, J. Kastner, R. Wenger, Metatracts-a method for robust extraction and visualization of carbon fiber bundles in fiber reinforced composites, in: 2015 IEEE Pacific Visualization Symposium (PacificVis), IEEE, pp. 191–198.

[6] J. Weissenböck, A. Amirkhanov, W. Li, A. Reh, A. Amirkhanov, E. Gröller, J. Kastner, C. Heinzl, Fiberscout: an interactive tool for exploring and analyzing fiber reinforced polymers, in: 2014 IEEE Pacific Visualization Symposium, IEEE, pp. 153–160. doi:10.1109/PacificVis.2014.52.

[7] G. Requena, G. Fiedler, B. Seiser, P. Degischer, M. Di Michiel, T. Buslaps, 3D-Quantification of the distribution of continuous fibres in unidirectionally reinforced composites, Composites Part A: Applied Science and Manufacturing 40 (2) (2009) 152–163. doi:10.1016/j.compositesa.2008.10.014.

[8] G. Seon, Y. Nikishkov, A. Makeev, B. Shonkwiler, Mesh morphing methodology for strength predictions in composites, Composite Structures 140 (2016) 612–620. doi:10.1016/j.compstruct.2015.12.021.

[9] O. Wirjadi, K. Schladitz, P. Easwaran, J. Ohser, Estimating fibre direction distributions of reinforced composites from tomographic images, Image Analysis & Stereology 35 (3) (2016) 167–179. doi:10.5566/ias.1489.

[10] J. Kastner, B. Plank, A. Reh, D. Salaberger, C. Heinzl, Advanced X-ray tomographic methods for quantitative characterisation of carbon fibre reinforced polymers, 4th International Symposium on NDT in Aerospace.

[11] S. C. Garcea, Y. Wang, P. J. Withers, X-ray computed tomography of polymer composites, Composites Science and Technology 156 (2018) 305–319. doi:10.1016/j.compscitech.2017.10.023.

[12] R. A. Smith, L. J. Nelson, M. J. Mienczakowski, P. D. Wilcox, Ultrasonic tracking of ply drops in composite laminates, in: AIP Conference Proceedings, Vol. 1706, AIP Publishing, 2016, p. 050006. doi:10.1063/1.4940505.

[13] L. J. Nelson, R. A. Smith, Three-dimensional fiber-orientation characterisation in monolithic carbon-fiber composites, in: Proc. European Conference on NDT, 2014.

[14] R. A. Smith, L. J. Nelson, M. J. Mienczakowski, R. E. Challis, Automated analysis and advanced defect characterisation from ultrasonic scans of composites, Insight-Non-Destructive Testing and Condition Monitoring 51 (2) (2009) 82–87.

[15] A. Sandhu, T. J. Dodwell, R. Butler, An autommated processing algorithm to determine wrinkle characteristics from B-scans, in: ECCM17 - 17th European Conference on Composite Materials, 2016.

[16] D. Pain, B. W. Drinkwater, Detection of fibre waviness using ultrasonic array scattering data, Journal of Nondestructive Evaluation 32 (3) (2013) 215–227.

[17] F. Prade, F. Schaff, S. Senck, P. Meyer, J. Mohr, J. Kastner, F. Pfeiffer, Nondestructive characterization of fiber orientation in short fiber reinforced polymer composites with X-ray vector radiography, NDT&E International 86 (2017) 65–72. doi:10.1016/j.ndteint.2016.11.013.

[18] R. A. Smith, L. J. Nelson, M. J. Mienczakowski, P. D. Wilcox, Ultrasonic analytic-signal responses from polymer-matrix composite laminates, IEEE Transactions on Ultrasonics, Ferroelectrics, and Frequency Control 65 (2) (2018) 231–243. doi:10.1109/TUFFC.2017.2774776.

[19] R. A. Smith, Use of 3D ultrasound data sets to map the localised properties of fibre-reinforced composites, Ph.d. (2010).

[20] R. A. Smith, L. J. Nelson, M. J. Mienczakowski, Phononic band gaps and phase singularities in the ultrasonic response from toughened composites., in: 2017 Review of Progress in Quantitative NDE, AIP Publishing, 2018.

[21] R. Smith, L. Nelson, R. T. Boumda, N. Xie, C. Fraij, P. Wilcox, S. Hallett, Progress in nondestructive 3D characterization and modelling of aerospace composites, in: NDT of Composites II, ASNT, pp. 38–44.

[22] L. Nelson, R. Smith, M. Mienczakowski, Ply-orientation measurements in composites using structure-tensor analysis of volumetric ultrasonic data, Composites Part A: Applied Science and Manufacturing 104 (2018) 108–119. doi:10.1016/j.compositesa.2017.10.027.

[23] X. Wu, X. Janson, Directional structure tensors in estimating seismic structural and stratigraphic orientations, Geophysical Journal International 210 (1) (2017) 534–548. doi:10.1093/gji/ggx194.

[24] X. Wu, D. Hale, 3D seismic image processing for unconformities, Geophysics 80 (2) (2015) IM35–IM44. doi:10.1190/GEO2014-0323.1.

[25] M. Krause, J.-M. Hausherr, B. Burgeth, C. Herrmann, W. Krenkel, Determination of the fibre orientation in composites using the structure tensor and local X-ray transform, Journal of Materials Science 45 (4) (2010) 888. doi:10.1007/s10853-009-4016-4.

[26] M. Axelsson, Estimating 3D fibre orientation in volume images, in: Pattern Recognition, 2008. ICPR 2008. 19th International Conference on, IEEE, 2008, pp. 1–4.

[27] R. S. J. Estépar, Local structure tensor for multidimensional signal processing: applications to medical image analysis, Presses univ. de Louvain, 2007.

[28] Z. Yu, C. Bajaj, A structure tensor approach for 3D image skeletonization: Applications in protein secondary structure analysis, in: Image Processing, 2006 IEEE International Conference on, IEEE, pp. 2513–2516.

[29] N. J. Schaub, S. J. Kirkpatrick, R. J. Gilbert, Automated methods to determine electrospun fiber alignment and diameter using the Radon transform, BioNanoScience 3 (3) (2013) 329–342. doi:10.1007/s12668-013-0100-y.

[30] M. Krause, R. M. Alles, B. Burgeth, J. Weickert, Retinal vessel detection via second derivative of local Radon transform, Universitat des Saarlandes Technical Report No. 212.http://www.math.uni-sb.de/service/preprints/preprint212.pdf.

[31] R. Smith, L. Nelson, N. Xie, C. Fraij, S. Hallett, Progress in 3D characterisation and modelling of monolithic carbon-fibre com-

posites, Insight-Non-Destructive Testing and Condition Monitoring 57 (3) (2015) 131–139. doi:10.1784/insi.2014.57.3.131.

[32] K. Jafari-Khouzani, H. Soltanian-Zadeh, Radon transform orientation estimation for rotation invariant texture analysis, IEEE Transactions on Pattern Analysis and Machine Intelligence 27 (6) (2005) 1004–1008.

[33] L. C. Lins, F. Wianny, S. Livi, C. Dehay, J. Duchet-Rumeau, J.-F. Gérard, Effect of polyvinylidene fluoride electrospun fiber orientation on neural stem cell differentiation, Journal of Biomedical Materials Research Part B: Applied Biomaterials 105 (8) (2017) 2376–2393.

[34] M. Tunák, J. Antoch, J. Kula, J. Chvojka, Estimation of fiber system orientation for nonwoven and nanofibrous layers: local approach based on image analysis, Textile Research Journal 84 (9) (2014) 989–1006. doi:10.1177/0040517513509852.

[35] K. K. Kratmann, M. Sutcliffe, L. Lilleheden, R. Pyrz, O. T. Thomsen, A novel image analysis procedure for measuring fibre misalignment in unidirectional fibre composites, Composites Science and Technology 69 (2) (2009) 228–238. doi:10.1016/j.compscitech.2008.10.020.

[36] C. Ayres, G. L. Bowlin, S. C. Henderson, L. Taylor, J. Shultz, J. Alexander, T. A. Telemeco, D. G. Simpson, Modulation of anisotropy in electrospun tissue-engineering scaffolds: analysis of fiber alignment by the fast Fourier transform, Biomaterials 27 (32) (2006) 5524–5534. doi:10.1016/j.biomaterials.2006.06.014.

[37] H. Heuer, M. Schulze, M. Pooch, S. Gäbler, A. Nocke, G. Bardl, C. Cherif, M. Klein, R. Kupke, R. Vetter, Review on quality assurance along the CFRP value chain–non-destructive testing of fabrics, preforms and CFRP by HF radio wave techniques, Composites Part B: Engineering 77 (2015) 494–501. doi:10.1016/j.compositesb.2015.03.022.

[38] R. Smith, L. Nelson, Composite evaluation, US. pat. 8,675,990.

[39] K. Schladitz, A. Büter, M. Godehardt, O. Wirjadi, J. Fleckenstein, T. Gerster, U. Hassler, K. Jaschek, M. Maisl, U. Maisl, Non-destructive characterization of fiber orientation in reinforced SMC as input for simulation based design, Composite Structures 160 (2017) 195–203. doi:10.1016/j.compstruct.2016.10.019.

[40] M. Sutcliffe, S. Lemanski, A. Scott, Measurement of fibre waviness in industrial composite components, Composites Science and Technology 72 (16) (2012) 2016–2023. doi:10.1016/j.compscitech.2012.09.001.

[41] C. Creighton, M. Sutcliffe, T. Clyne, A multiple field image analysis procedure for characterisation of fibre alignment in composites, Composites Part A: Applied Science and Manufacturing 32 (2) (2001) 221–229.

[42] S. Dietrich, J.-M. Gebert, G. Stasiuk, A. Wanner, K. Weidenmann, O. Deutschmann, I. Tsukrov, R. Piat, Microstructure characterization of CVI-densified carbon/carbon composites with various fiber distributions, Composites Science and Technology 72 (15) (2012) 1892–1900.

[43] O. Wirjadi, K. Schladitz, A. Rack, T. Breuel, Applications of anisotropic image filters for computing 2D and 3D-fiber orientations, in: Stereology and Image Analysis–10th European Congress of ISS.

[44] K. Robb, O. Wirjadi, K. Schladitz, Fiber orientation estimation from 3D image data: practical algorithms, visualization, and interpretation, in: 7th international conference on hybrid intelligent systems (HIS 2007), IEEE, pp. 320–325. doi:10.1109/HIS.2007.26.

[45] A. Ayadi, H. Nouri, S. Guessasma, F. Roger, Determination of orthotropic properties of glass fibre reinforced thermoplastics using X-ray tomography and multiscale finite element computation, Composite Structures 136 (2016) 635–649.

[46] H. Altendorf, D. Jeulin, 3D directional mathematical morphology for analysis of fiber orientations, Image Analysis & Stereology 28 (3).

[47] H. Altendorf, E. Decencière, D. Jeulin, P. Peixoto, A. Deniset-Besseua, E. Angelini, G. Mosser, M.-C. Schanne-Klein, Imaging and 3D morphological analysis of collagen fibrils, Journal of microscopy 247 (2) (2012) 161–175.

[48] J. Radon, On the determination of functions from their integral values along certain manifolds, IEEE Transactions on Medical Imaging 5 (4) (1986) 170–176. doi:10.1109/TMI.1986.4307775.

[49] M. Van Ginkel, C. L. Hendriks, L. J. Van Vliet, A short introduction to the Radon and Hough transforms and how they relate to each other, Delft University of Technology Quantitative Imaging Group Technical Report Series (2004).

[50] V. A. Shapiro, V. I. Kavardjikov, S. A. Atanassov, Approach to automatic analysis of Young's fringes in speckle photography, Applied optics 32 (23) (1993) 4378–4387.

[51] Q. Kemao, A. Asundi, Characterizing Young's fringes' orientation and spacing by Fourier transform and Radon transform, Optics & Laser Technology 34 (7) (2002) 527–532.

[52] M. R. Hejazi, Y.-S. Ho, Texture analysis using modified discrete Radon transform, IEICE Transactions on Information and Systems 90 (2) (2007) 517–525.

[53] ASM handbook. Volume 17, Nondestructive evaluation and quality control, Metals Park, Ohio : ASM International, 1989.